

# Caking-Inspired Cold Sintering of Plastic Supramolecular Films as Multifunctional Platforms

Mengqi Xie, Yuxuan Che, Kaerdun Liu, Lingxiang Jiang, Limin Xu, Rongrong Xue, Markus Drechsler, Jianbin Huang, Ben Zhong Tang, and Yun Yan\*

Caking of powder materials is undesired in various industries, and for thousands of years people are fighting against caking. Herein, the principle of caking is employed to create macroscopic plastic supramolecular films through a cold sintering process. A nanometer-sized, irregular coordinating cluster is first generated with a bulky head surfactant and multifunctional ligand, and the addition of metal ions immediately leads to amorphous white precipitates. Upon adsorbing moisture, a rearrangement of the molecules in the precipitates results in cold sintering, so that the particles in the precipitates grow into a transparent macroscopic film. The mechanical strength of the film is comparable to plastics, but allows welding and molding with finger at ambient temperature in moist environment. Mechanical tests suggest the supramolecular plastic does not fatigue even after several tens circles' remolding, indicating their superior material engineering capability. This strategy can be extended to different chemistries to fabricate films with different mechanical strength. Various functional components can be doped into the resultant films, rendering them a platform toward multifunctional materials, such as luminescent devices or sensors for pollution gases. The current strategy opens up a new vista in material science is expected.

## 1. Introduction

Many powder materials can undergo deliquescence to form a large cake, which is undesired because caking may generate a negative impact on the service reliability and the storage lifetime of these materials. The reason for caking in powder materials is the moisture-triggered rearrangement of molecules to form bridges between particles.<sup>[1]</sup> The moisture absorbing ability for a material may either originate from the presence of hygroscopic components, or form capillary effect generated by the gap between particles. Small particles with irregular shapes or heterogeneous sizes can experience drastic caking due to the large contact area. For thousands of years, people have been fighting against caking.

In contrast to the tremendous efforts devoted to anticaking, currently people are making a serious effort to fabricate bulk macroscopic materials, especially plastic films, to create synthetic advanced materials.<sup>[2]</sup> Thus far, the methodology of film formation mainly includes evaporation of organic solution of polymers, and thermal

molding of polymer melts.<sup>[2d,3]</sup> All these methods require considerable energy input, either for the removal of solvent, or for heating and cooling the polymeric materials. We postulate that if the principle of caking is positively utilized to fabricate macroscopic materials, plastic films may form as a result of spontaneous formation of bridges between nanometer-sized particles, which avoids the energy input for solvent evaporation or melting polymer blends, rendering significant energy economy. However, thus far, the simple principle of caking that utilizes the native tendency of forming interparticle bridges, has never been positively employed in material science.


Herein, we present our design of caking-inspired cold sintering of plastic films, as illustrated in **Scheme 1**, that are able to form instantly (within 10 s) under the press exerted with finger, or by themselves within 12 h. We first fabricate irregular ionic complexes in water using a bulky headed surfactant and an oppositely charged amphiphile possessing multicoordinating heads, followed by crosslinking the irregular ionic complexes into precipitates via metal coordination. Physically adsorbed water in the precipitates drives rearrangement of the directional coordination bonds between the ionic complexes,

M. Xie, Y. Che, K. Liu, Dr. L. Xu, R. Xue, Prof. J. Huang, Prof. Y. Yan  
Beijing National Laboratory for Molecular Sciences (BNLMS)  
College of Chemistry and Molecular Engineering  
Peking University  
Beijing 100871, China  
E-mail: yunyan@pku.edu.cn

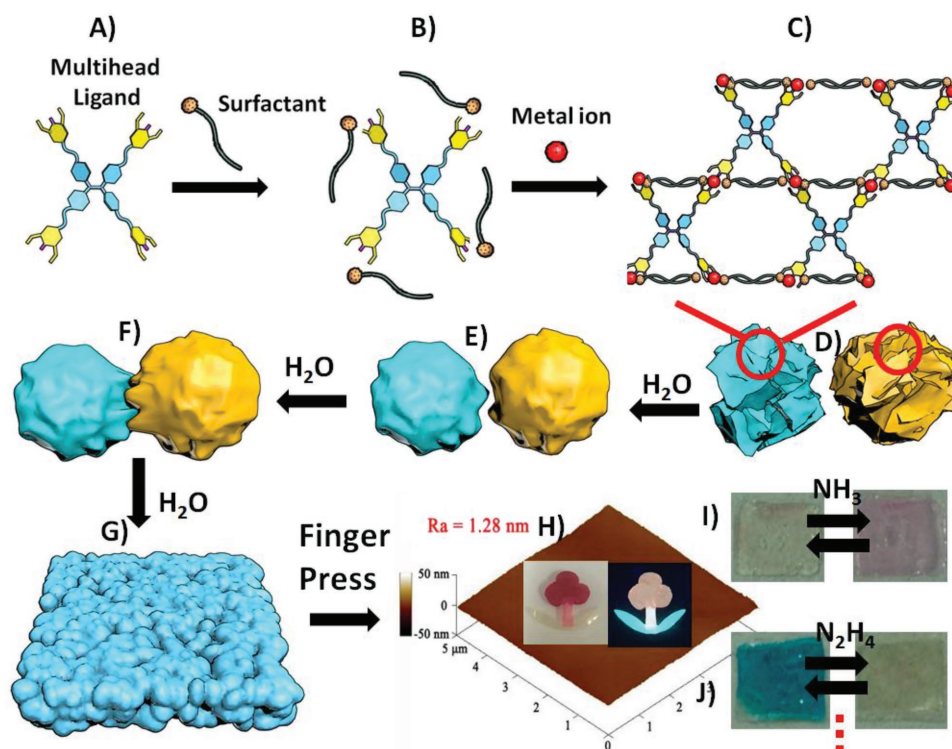
Prof. L. Jiang  
College of Chemistry and Materials Science  
Jinan University  
Guangzhou 510632, China

Dr. M. Drechsler  
Bayreuth Institute of Macromolecular Research (BIMF)-TEM  
University of Bayreuth  
Universitätsstrasse 30, D-95440 Bayreuth, Germany

Prof. B. Z. Tang  
Department of Chemistry  
Division of Biomedical Engineering  
Hong Kong University of Science and Technology  
Clear Water Bay, Kowloon, Hong Kong, China

 The ORCID identification number(s) for the author(s) of this article can be found under <https://doi.org/10.1002/adfm.201803370>.

DOI: 10.1002/adfm.201803370



**Scheme 1.** Illustration of the caking-inspired cold sintering of macroscopic plastic supramolecular film. H<sub>2</sub>O in the scheme represents water absorbed from moisture environment. A–C) are the illustrations of the interaction at molecular scale. D) represents the irregular particles formed through process. D–G) illustrations of moisture-triggered gradual changes of the particles at a microscopic scale. The particles are labeled in cyan and yellow to show the gradual formation of the bridges between them. H) shows the AFM image of the bulk film and (G) pressed by fingers through a glass slide. The insets in (H) are the art images made with the pressed film by welding different films under moisture in daylight and under 365 nm UV light. The red color for the flower is from the doped fluorescent dye of rhodamine B, while the blue–green fluorescence of the leaves is from the multihead ligand. I) and J) show the film can be made into sensors for NH<sub>3</sub> and N<sub>2</sub>H<sub>4</sub> when proper dyes are imbedded.

leading to robust, self-supporting, transparent macroscopic films with useful mechanical properties that are analogous to polymeric plastics, but capable of engineering at ambient condition. This strategy can be extended to different chemistries, and many functional components can be doped into the film facily during the precipitation process. We demonstrate that by doping various dyes the film may be used to construct luminescence device or sensors for the detection of specific pollution gas. We expect the strategy of caking inspired cold sintering may open up a new vista in material science.

## 2. Results and Discussion

### 2.1. Metallosupramolecular Powder

Figure 1 shows the system that we employed to construct the caking-inspired cold sintering of plastic films, which is composed of the hygroscopic surfactant dodecyl ammonium triethyl ammonium bromide (DEAB), the four-armed amphiphile TPE-BPA, and Zn(NO<sub>3</sub>)<sub>2</sub>. These three single components are all highly soluble in water, and the TPE-BPA can coordinate with Zn<sup>2+</sup> ions and electrostatically interact with the DEAB. The employment of hygroscopic DEAB is to ensure that the molecules in the resultant material are capable of adsorbing moisture. Meanwhile, the bulky triethyl head also prohibits the molecules in the material

from packing densely,<sup>[4]</sup> which is beneficial for the rearrangement of the molecules. TPE-BPA (Scheme 1 and Figure 1) is a propeller-shaped molecule due to the presence of its tetra-phenyl ethylene (TPE) core. The structural mismatch between DEAB and TPE-BPA allows the formation of irregular ionic nanoclusters in water, which is different from the well-defined self-assembly of ionic complexes formed with planar molecules.<sup>[5]</sup> Figure 1d,e shows that the electrostatic interaction between DEAB and TPE-BPA results in an enhancement of the fluorescence due to the aggregation-induced emission of the TPE group.<sup>[6]</sup> Cryogenic transmission electronic microscopy (Cryo-TEM) observations reveal the formation of irregular clusters with an average size of approximately 13 nm at the composition corresponding to the strongest fluorescence (Figure 1h and Figure S1, Supporting Information). Since each Zn<sup>2+</sup> ion may coordinate with two heads of the TPE-BPA,<sup>[7]</sup> the addition of Zn(NO<sub>3</sub>)<sub>2</sub> to the fluorescent systems immediately causes precipitation (Figure 1f and Figure S2, Supporting Information) as a result of the coordination-triggered crosslinking of the irregular TPE-BPA/DEAB clusters. The fresh precipitates are amorphous white powders, which display the characteristic blue–green emission of the TPE moiety (Figure 1g).<sup>[8]</sup> The elemental analysis shows that the precipitate is composed of DEA<sup>+</sup>:TPE-BPA<sup>8-</sup>:Zn<sup>2+</sup> at a molar ratio of 4:1:2 (Table S1, Supporting Information), suggesting the formation of a charge neutral composite. X-ray photoelectron spectroscopy (XPS) (Figure S3, Supporting Information) and Fourier

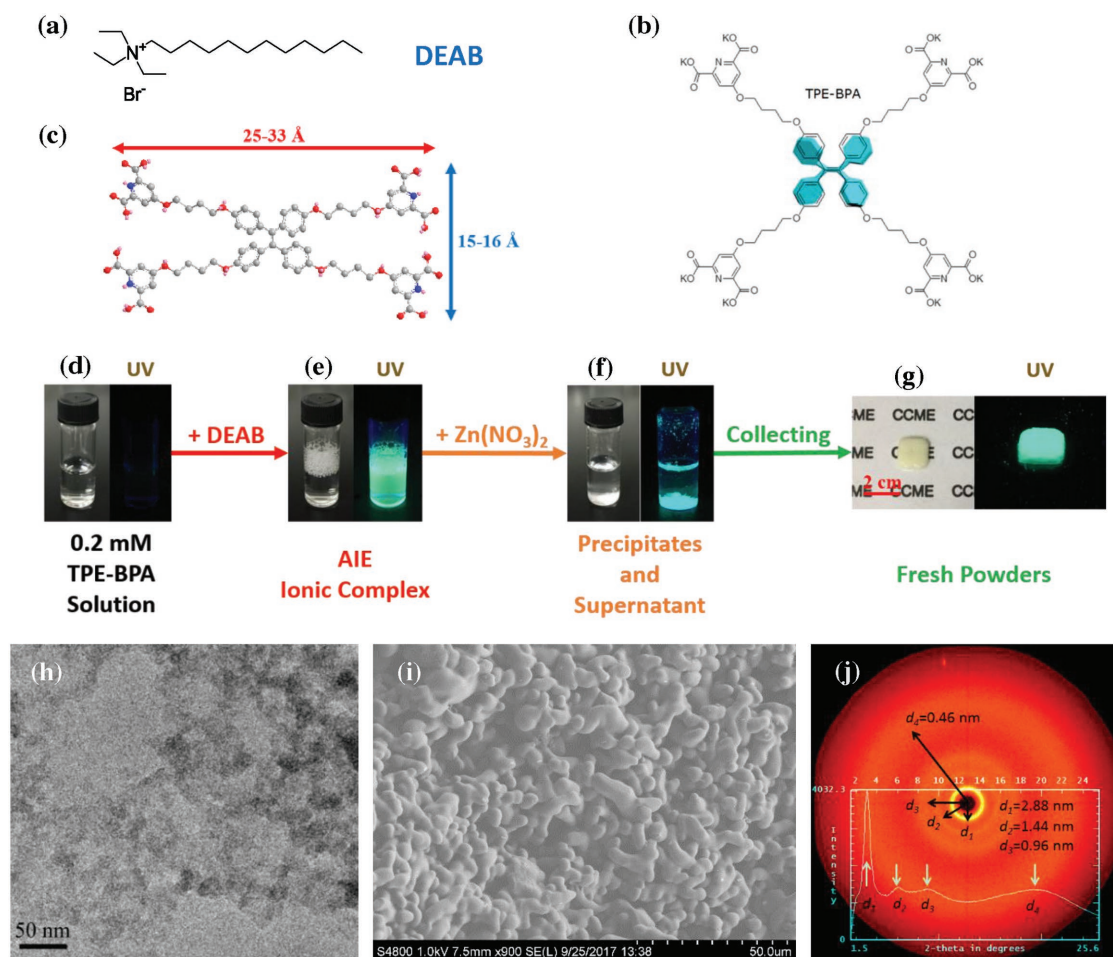


**Figure 1.** a) Molecular structure of DEAB, b) TPE-BPA, and its geometry (c) obtained using a Gaussian calculation. The lengths along the long and short axes are labeled. Because the benzene ring may rotate around the ethylene plane, both lengths may vary within a certain range. d–g) are photos of the aqueous system of TPE-BPA (d), the TPE-BPA/DEAB (e), TPE-BPA/DEAB/ $Zn(NO_3)_2$ , and (f) the fresh amorphous powder of TPE-BPA/DEAB/ $Zn(NO_3)_2$  under daylight and 365 nm UV light (g). h) ( $[TPE-BPA] = 0.2 \times 10^{-3} M$ ,  $[DEAB] = 3.2 \times 10^{-3} M$ ,  $[Zn(NO_3)_2] = 0.2 \times 10^{-3} M$ ), a Cryo-TEM image of the irregular nanoclusters formed by TPE-BPA/DEAB in solution. i) SEM image of the fresh, amorphous precipitates of TPE-BPA/DEAB/ $Zn(NO_3)_2$ . j) 2D XRD image of the precipitates. The inset in (j) is the normal XRD image of the precipitates.

transform infrared spectroscopy (FT-IR) (Figure S4, Supporting Information) measurements reveal that the  $Zn^{2+}$  ion coordinates to the ligand head of TPE-BPA.

The morphology of the powder precipitates is comprised of connected spheres, as revealed by scanning electron microscopy (SEM) (Figure 1i) and transmission electron microscopy (TEM) (Figure S5, Supporting Information), which is in drastic contrast to the irregular cluster morphology of TPE-BPA/DEAB. This indicates that the coordination with  $Zn^{2+}$  ions triggers the rearrangement of the TPE-BPA and DEAB molecules. Small-angle X-ray scattering (SAXS, Figure S6, Supporting Information) and two-dimensional X-ray diffraction (2D XRD) (Figure 1j) studies of the precipitate reveal three diffraction peaks with distances of 2.88, 1.44, and 0.96 nm (Figure 1j), which are characteristic of well-ordered, layered structures. The lamellar period of 2.88 nm is in good agreement with the length of the long axis of TPE-BPA obtained from Gaussian calculation (Figure 1c), indicating the presence of TPE-BPA layers in the precipitate. These TPE-BPA layers are randomly oriented in the precipitates, as indicated by the fact that the 2D XRD pattern (Figure 1j) appears as concentric rings. No individual diffractions of DEAB

(Figure S7, Supporting Information) were observed in the precipitates, and no ordered packing of the alkyl chain of DEAB was revealed in the FT-IR spectra (Figure S8, Supporting Information). Furthermore, two-dimensional hydrogen-1 nuclear magnetic resonance spectroscopy ( $2D^1H$ NMR) measurements suggests no correlation between the protons in the hydrocarbon portion of DEAB and TPE-BPA (Figure S9, Supporting Information). All these results suggested that the DEAB molecules were embedded in the plane formulated by the TPE-BPA layers. The perpendicular alignment of the DEAB chains to the TPE-BPA plane (Figure S10, Supporting Information) is ruled out by the presence of only one period corresponding to the TPE-BPA molecule. Such a random packing of alkyl chains results in a broad diffuse ring in the wide-angle region of the 2D XRD spectra (or a broad peak in the XRD spectra).

## 2.2. Caking-Inspired Film Formation

Since DEAB is a hygroscopic surfactant, we speculate the powder material may undergo cold sintering to form a bulk

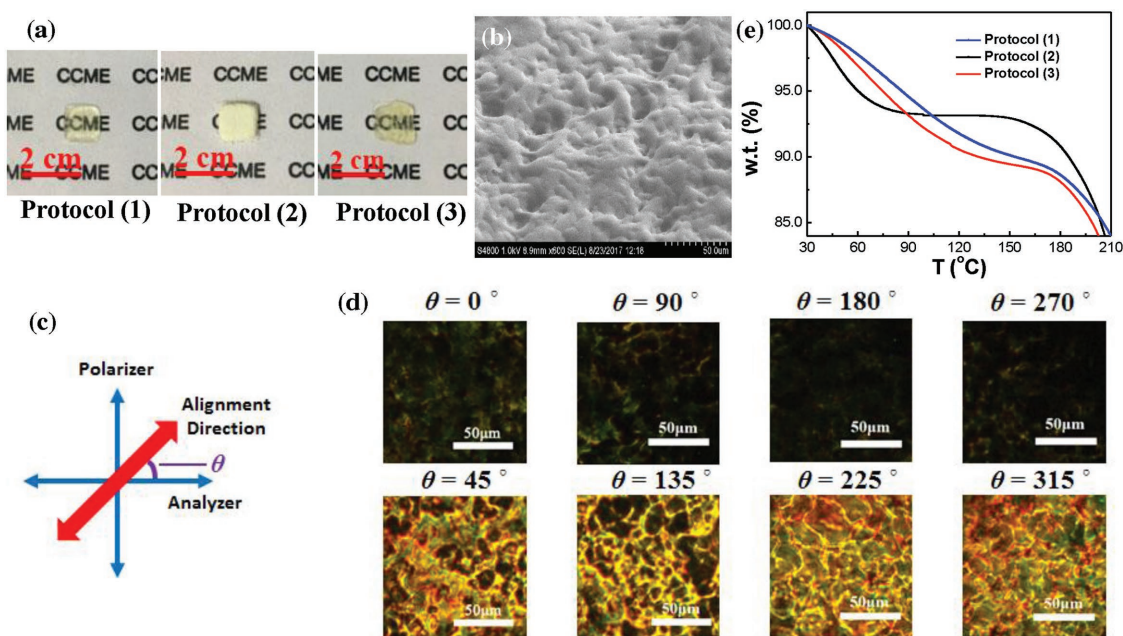


**Figure 2.** a) Photos of the transparent film and the amorphous powder precipitates processed through protocols (1), (2), and (3). b) SEM image of the film's surface. c,d) POM images of the transparent film. c) illustrates the alignment direction of the film in between two polarizers. (e) TGA results for the powder precipitates and the transparent films (30–210  $^\circ\text{C}$ ).

macroscopic solid upon exposure to moisture as a result of the rearrangement of the coordination bridges between the particles. To test this hypothesis, the white precipitate was treated in three parallel ways: 1) it was incubated in a humid environment; 2) it was kept in a dry environment after being vacuum dried; and 3) it was subjected to moisture after being vacuum dried. Excitingly, bulk, colorless, transparent films were obtained within 2 h for conditions (1) and (3), whereas the precipitates in (2) were still white powders (Figure 2a), which qualitatively confirmed the occurrence of a rearrangement of the coordinating bonds. The SAXS (Figure S6, Supporting Information) and 2D XRD measurements (Figure S11, Supporting Information) revealed that the diffraction patterns from the powder precipitates and the transparent films were the same and confirmed that they have the same molecular packing mode. SEM observation showed that the films have connecting structures with a bumpy surface (Figure 2b), while the TEM study showed that the cross-section displays featureless details (Figure S12, Supporting Information), indicating the formation of a homogenous macroscopic structure. The sizes of the ordered domains of the powder precipitate and the transparent films are similar, as estimated from the half-height widths of the SAXS peaks that were determined using the Scherrer equation (Methods section in Supporting Information). This means that cold sintering indeed occurred in the amorphous powders, and the formation of transparent film is a result of vanishing of the boundaries between particles owing to the formation of coordinating bridges between them.

No stripes (aligned from metal ions)<sup>[3a,9]</sup> were observed in the films under high-resolution TEM, which suggested that the coordinating centers were not well aligned. This is understandable because the propeller-shaped TPE-BPA molecule cannot undergo sufficient  $\pi$ - $\pi$  stacking. Albeit it lacked the stacking

of TPE-BPA, the transparent film still displayed birefringence in the polarized optical microscopy (POM). Figure 2c,d demonstrates the POM image of the transparent film observed at different angles in between two vertically aligned polarizers. Strong extinction occurs at the angle of  $0^\circ$ ,  $90^\circ$ ,  $180^\circ$ , and  $270^\circ$ , whereas the brightest birefringence is observed at  $45^\circ$ ,  $135^\circ$ ,  $225^\circ$ , and  $315^\circ$ , indicating the smectic liquid crystal nature of the transparent film. It is noticed that domains of several micrometers can be clearly identified from different colors, suggesting the film are composed of connected mesoscopic smectic liquid crystal phases. Similar POM images are observed for films made both by protocols 1 and 3 (Figure S13, Supporting Information), indicating that the molecules were well oriented in the film. In contrast, the powder precipitates do not display birefringence (Figure 2d) due to the presence of particle boundaries that reflect and scatter the incident light in diverse directions.

The thermogravimetric analysis (TGA) measurements (Figure 2e) suggest that the water content of the film is approximately 10%, regardless of the protocols used to produce it. The dried powders contain 7% water (which can be lost at approximately 80  $^\circ\text{C}$ ), indicating they are physically adsorbed water. Obviously, the additional 3% water is very crucial in triggering the rearrangement of the coordinating bonds. If the water in the films can be considered as crystal water, detailed calculation reveals that the composition of the wet and dried film is  $4\text{DEA}^+ \cdot \text{TPE-BPA}^{8-} \cdot 2\text{Zn}^{2+} \cdot 16\text{H}_2\text{O}$  and  $4\text{DEA}^+ \cdot \text{TPE-BPA}^{8-} \cdot 2\text{Zn}^{2+} \cdot 11\text{H}_2\text{O}$ , respectively.

Strikingly, the formation of transparent films can be promoted by pressing, i.e., similar to molding polymer melts into films.<sup>[10]</sup> We found that upon exerting a pressure of approximately 0.7 MPa with finger through a glass slide, the cake of white powder transforms into a transparent film within 10 s

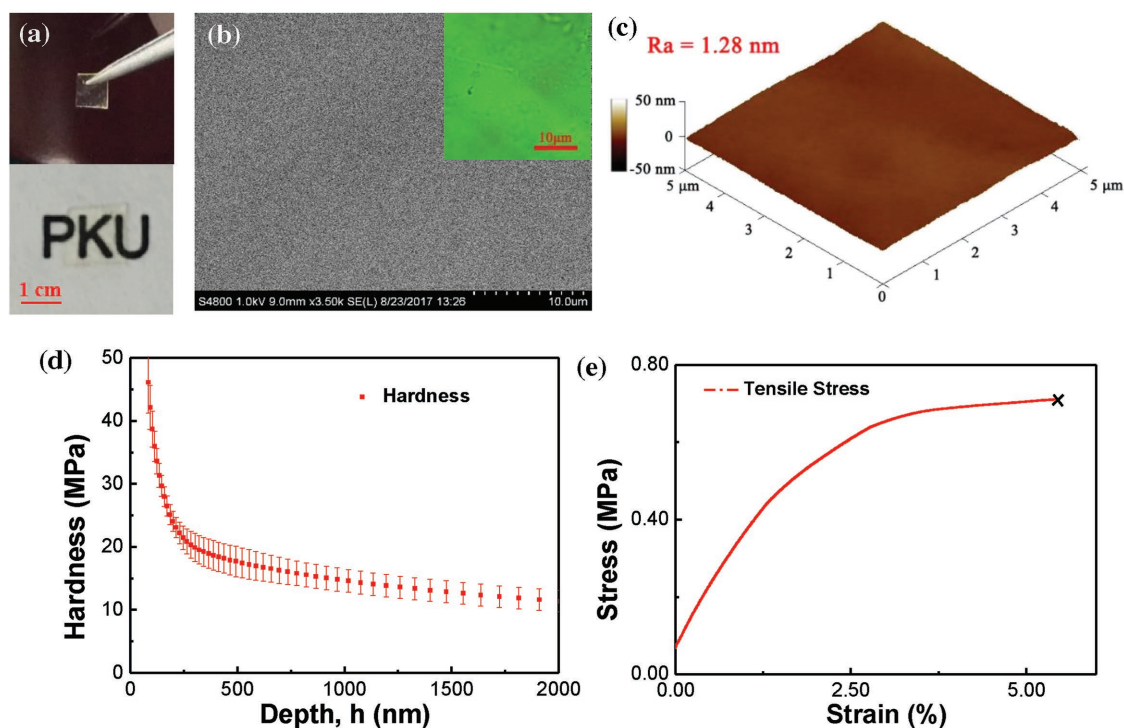


**Figure 3.** a) Photos of the transparent film formed by pressing the fresh precipitates under a pressure of 0.7 MPa for 10 s. b) SEM and c) AFM images of the pressed film. The inset in (b) is the POM image of the pressed film. d, e) are the mechanical tests for the hardness and tensile stress of the film.

(Figure 3a). The surface of the resultant film is very smooth (with roughness  $R_a \approx 1.28$  nm) according to SEM and atomic force microscopy (AFM) (Figure 3b,c), and the birefringence under POM is featureless, indicating a homogeneous film thickness (inset in Figure 3b). Mechanical tests (Figure 3d,e) reveal the hardness of film is about  $15 \pm 2$  MPa, with a tensile strength of  $0.65 \pm 0.16$  MPa, Young's Modulus of  $20.7 \pm 10.7$  MPa, and toughness of  $2.9 \pm 2.8 \times 10^4$  J m<sup>-3</sup>. These parameters suggest that the film has a feature of plastic material.

The TGA analysis reveals that the water content of the pressed film is also approximately 10% (Figure S14, Supporting Information), and the SAXS and 2D XRD patterns of the film are the same as those obtained with protocols 1, 2, and 3 (Figures S6 and S15, Supporting Information). The differential scanning calorimeter (DSC) measurements show that all the films have no obvious phase-transition temperature in the range of 10–140 °C (Figure S16, Supporting Information), and the organic components decompose above 150 °C. It is possible that the nanocluster domains in these materials are not large enough to result in a phase transition.

### 2.3. Processable Plastic Films

The ability to absorb moisture of the transparent film allows welding two separated films together in moist environment. Instant welding of two separated pieces occurs within 10 s when pressed in a humid environment (Figure 4a). To demonstrate the success of the welding clearly, one film is labeled with the fluorescent dye rhodamine B, which was doped in the film by coprecipitation (Methods section). Figure 4b shows that two

separated films can adhere firmly to each other, either edge to edge or face to face. The three-dimensional confocal laser scanning microscopy (3D CLSM) observations (Figure 4c,d, and Figure S17a and S17b, Supporting Information) reveal that the edge-to-edge welding is complete throughout the depth of the cut. This load-enabled, instant welding makes it possible to mold the films into various topologies and patterns (Figure 4e). Especially, the remolding of damaged films in a moist environment can lead to a new film. The mechanical tests indicate that the new film has exactly the same mechanical properties as the original one (Figure 4f). The remolding tests can be repeated tens of times without changing the mechanical properties (Figure 4f), indicating the superior 100% reversibly engineering capacity of this supramolecular plastic film.

Although welding and molding of the film require sufficient moisture, the film remains integrated once it is formed, regardless of its moisture content. Even in the presence of water, the films remain intact (Figure S18, Supporting Information), indicating the constituent molecules have been firmly locked via coordination and ionic interaction in the film. Actually, a transparent film can be formed in water after centrifuging the suspended precipitates for 5 min at 5000 rpm. The photo shows the formation of a whole transparent film at the bottom of the test tube immediately after centrifugation (Figure S19, Supporting Information). It is noticed if the film is dried at about 100 °C, it becomes difficult to fold or stretch. Mechanical test suggests that the film breaks at a strain of 2%, while this occurs at about 15% for a wet film. However, the tensile strength of the film remains unchanged in both dried and wet states (Figure S20, Supporting Information).

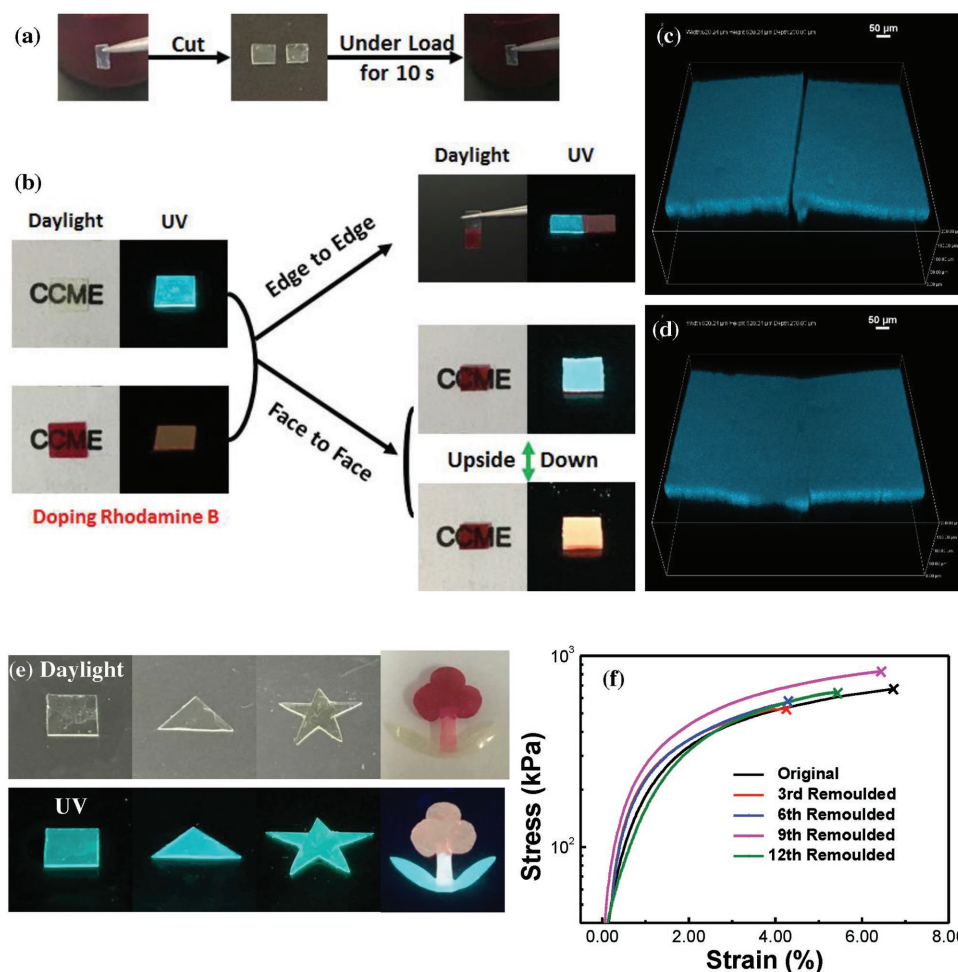


**Figure 4.** a) Photos of the welding of two pieces film under a load. b) Photos of the load-facilitated instant edge-to-edge and face-to-face adhesion of the films under daylight and 365 nm UV light. c, d) 3D CLSM images of the cuts on the films before (c) and after (d) edge-to-edge welding. e) Photos of the films in various topologies under daylight and 365 nm UV light. The flower is made by molding the native film and that doped with rhodamine B together under moist environment. f) Stress–strain curves of the films after experiencing different cycles of remolding.

## 2.4. Multifunctional Platforms

The sufficient mechanical strength and stability of the film allows doping different functional materials into it, rendering formation of a promising platform to create multifunctional materials. **Figure 5** shows that upon doping of rhodamine B in the TPE-BPA/DEAB/ $Zn^{2+}$  film, tunable emission ranging from blue–green to orange can be obtained, depending on the molar ratio of rhodamine B and TPE-BPA (Figure S21, Supporting Information). As these films are deposited on a ultra-violet light emitting diode (UV-LED) (Figure 5a,b), luminescent devices of diversified colors can be facilely fabricated. Alternatively, if we dope other dyes, such as phenolphthalein and methylthionine chloride, it allows generation of sensors that are able to detect pollution gases. The colorless film containing phenolphthalein will change into pink in  $NH_3$  atmosphere (Figure 5c), while the film with embedded methylthionine chloride will turn blue when exposed to the vapor of  $N_2H_4$  (Figure 5d). Both the two sensing processes are reversible. Figure 5e shows the absorption of phenolphthalein occurs reversibly without fatigue as the

sensing experiments are repeated for many circles. We expect that this strategy of caking inspired plastic film engineering can be extended to a wide variety of applications, even in the fabrication of electric skins.<sup>[24,11]</sup> Relevant work is ongoing in our lab, and will be reported later.

## 2.5. A Universal Strategy

It is worth noting that the strategy of caking-inspired cold sintering of plastic supramolecular material engineering is capable of being generalized to different chemistries. First, moisture-facilitated bridges between particles can be coordination bonds formed with other metal ions, such as  $Co^{2+}$ ,  $Ni^{2+}$ , or  $Cu^{2+}$  (Figures S22 and S23, Supporting Information). Second, the chemistry of the multifunctional ligand can be varied. If the TPE moiety is replaced with an azobenzene (Azo) group (Figure S24, Supporting Information), a film is also created, although the number of the coordinating arms is drastically reduced by onefold. Elemental analysis suggests

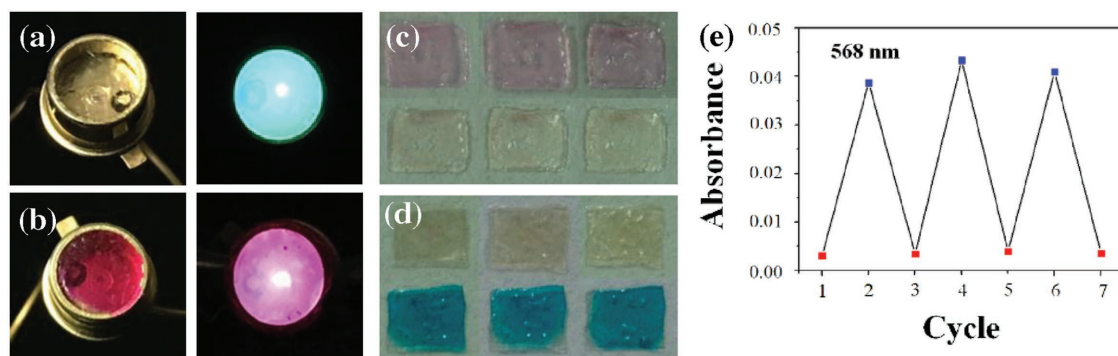


**Figure 5.** a,b) Photos of the UV-LEDs coated with the TPE-BPA/DEAB/Zn<sup>2+</sup> film (a) and with film doped with  $0.2 \times 10^{-3}$  M rhodamine B (b) under visible light (left) and 365 nm UV light (right). c,d) are the photos of the TPE-BPA/DEAB/Zn<sup>2+</sup> films doped with  $0.1 \times 10^{-3}$  M phenolphthalein and methylthionine chloride, respectively. The upper rows in (c) and (d) are the film before exposure to NH<sub>3</sub> and N<sub>2</sub>H<sub>4</sub>, whereas the lower rows are photos after exposure to the corresponding gases. The three films in each case show the photos after repeated exposure. e) is the absorbance of phenolphthalein at 568 nm before (red squares) and after (blue squares) exposure to NH<sub>3</sub>.

that a charge neutral film is formed as well, since the molar ratio between the Azo<sup>4-</sup>:DEA<sup>+</sup>:Zn<sup>2+</sup> = 1:2:1 (Figure S25 and Table S2, Supporting Information). Meanwhile, a lamellar structure with period of 3.3 nm (Figure S26, Supporting Information), corresponding to the extending length of the Azo ligand is obtained,<sup>[12]</sup> confirming the similar molecular arrangement to that in the TPE-BPA film. Third, the bridges between the particles are not necessarily coordination bonds. Since the carbonate groups at the coordinating head of dicarboxylate pyridine can form hydrogen bonds with hydroxyl groups, plastic films can form as well when the metal ions are replaced with tannic acid (Figures S27 and S28, Supporting Information). Fourth, the surfactant DEAB can be changed too. For instance, if DEAB is replaced by tripropyl-dodecylammonium bromide or tributyl-dodecylammonium bromide, similar films can be formed (Figure S29, Supporting Information). However, surfactant with smaller head, such as trimethyl-dodecylammonium bromide, and longer chains, such as cetyltriethylammonium bromide (Figures S30 and S31, Supporting Information) fail to lead to the formation of films. We assume that a looser molecular arrangement is necessary to rearrange the constituent molecules in a moist environment formation, while smaller head and long chains tend to create denser molecular aggregates. It is worth noting that the mechanical strength of the films formed with different chemistry is different. In the present study, the film formed with Azo group has better elastic properties (data not shown), suggesting the  $\pi$ - $\pi$  stacking between the planar azobenzene group, which is absent in the propeller-shaped TPE-BPA molecules, has contributed to the mechanical strength of the resultant film. This means, it is possible to generate films with desired mechanical properties by modifying the chemical structure of the ligand. It should be pointed out that variation of metal ions for a given ligand also impacts the mechanical ability of the film, since the equilibrium constant for the coordination between the ligand and metal ions differs. Interestingly, the film formation is possible as well if DEAB is added to the precipitates formed by TPE-BPA/Zn<sup>2+</sup> (Figures S32 and S33, Supporting Information). This confirms that the film formation is completely reversible and

the cold sintering is enabled by the surfactant facilitated rearrangement of molecules in the precipitates of coordination supramolecular polymers.

### 3. Conclusion

In summary, we proposed a caking-inspired cold sintering approach to prepare macroscopic solid supramolecular plastic films with the aid of coordination chemistry and surfactants. Compared with previous strategies, the caking-inspired film engineering positively utilizes the automatically occurred event of molecular rearrangement, so that the dependence on external energy input in fabricating plastic films is greatly reduced. We show that the amorphous precipitates of the ionic complex of surfactant/amphiphilic ligand cross-linked by coordination bond can be fabricated into transparent macroscopic films instantly. Many functional components can be doped into the film. In combination with the possibility of employing different chemistries, we expect that this strategy will allow the fabrication of various functional plastic materials, which will open up a new vista in material science.

### Supporting Information

Supporting Information is available from the Wiley Online Library or from the author.

### Acknowledgements

This work was financially supported by the National Natural Science Foundation of China (NSFC21573011 and 21422302). Grant no. NSFC 21633002. The authors appreciate very much the help of Dr. Yifan Zhang from Center for Soft and Living Matter, Institute for Basic Science (IBS), Ulsan 44919, Republic of Korea, for the kindest help in design of the cover image for this paper.

### Conflict of Interest

The authors declare no conflict of interest.

## Keywords

caking, cold sintering, coordination, multifunctional platform, supramolecular films

Received: May 15, 2018

Revised: June 9, 2018

Published online:

- [1] a) J. Aguilera, J. del Valle, M. Karel, *Trends Food Sci. Technol.* **1995**, 6, 149; b) L. J. Mauer, L. S. Taylor, *Pharm. Dev. Technol.* **2010**, 15, 582; c) M. Peleg, A. M. Hollenbach, *Food Technol.* **1984**, 38, 93; d) B. Provent, D. Chulia, J. Cary, *Eur. J. Pharm. Biopharm.* **1993**, 39, 202.
- [2] a) J. Cao, C. Lu, J. Zhuang, M. Liu, X. Zhang, Y. Yu, Q. Tao, *Angew. Chem., Int. Ed.* **2017**, 56, 8795; b) E. D'Elia, S. Barg, N. Ni, V. G. Rocha, E. Saiz, *Adv. Mater.* **2015**, 27, 4788; c) Y. Sun, J. Lopez, H. W. Lee, N. Liu, G. Zheng, C. L. Wu, J. Sun, W. Liu, J. W. Chung, Z. Bao, *Adv. Mater.* **2016**, 28, 2455; d) B. C. Tee, C. Wang, R. Allen, Z. Bao, *Nat. Nanotechnol.* **2012**, 7, 825.
- [3] a) M. Burnworth, L. Tang, J. R. Kumpfer, A. J. Duncan, F. L. Beyer, G. L. Fiore, S. J. Rowan, C. Weder, *Nature* **2011**, 472, 334; b) D. J. Lunn, O. E. Gould, G. R. Whittell, D. P. Armstrong, K. P. Mineart, M. A. Winnik, R. J. Spontak, P. G. Pringle, I. Manners, *Nat. Commun.* **2016**, 7, 12371.
- [4] a) Y. Yan, W. Xiong, J. B. Huang, Z. C. Li, X. S. Li, N. N. Li, H. L. Fu, *J. Phys. Chem. B* **2005**, 109, 357; b) Y. Yan, W. Xiong, X. S. Li, T. Lu, J. B. Huang, Z. C. Li, H. L. Fu, *J. Phys. Chem. B* **2007**, 111, 2225.
- [5] a) M. Antonietti, J. Conrad, A. Thuenemann, *Macromolecules* **1994**, 27, 6007; b) C. F. J. Faul, M. Antonietti, *Adv. Mater.* **2003**, 15, 673; c) K. Binnemans, *Chem. Rev.* **2005**, 105, 4148.
- [6] a) J. Mei, N. L. C. Leung, R. T. K. Kwok, J. W. Y. Lam, B. Z. Tang, *Chem. Rev.* **2015**, 115, 11718; b) L. J. Chen, Y. Y. Ren, N. W. Wu, B. Sun, J. Q. Ma, L. Zhang, H. W. Tan, M. H. Liu, X. P. Li, H. B. Yang, *J. Am. Chem. Soc.* **2015**, 137, 11725; c) X. Z. Yan, M. Wang, T. R. Cook, M. M. Zhang, M. L. Saha, Z. X. Zhou, X. P. Li, F. H. Huang, P. J. Stang, *J. Am. Chem. Soc.* **2016**, 138, 4580.
- [7] a) Y. Yan, N. A. M. Besseling, A. de Keizer, A. T. M. Marcelis, M. Drechsler, M. A. Cohen Stuart, *Angew. Chem., Int. Ed.* **2007**, 46, 1807; b) Y. Yan, A. A. Martens, N. A. M. Besseling, F. A. de Wolf, A. de Keizer, M. Drechsler, M. A. Cohen Stuart, *Angew. Chem., Int. Ed.* **2008**, 47, 4192; c) Y. Yan, J. Huang, *Coord. Chem. Rev.* **2010**, 254, 1072.
- [8] a) Y. Q. Dong, J. W. Y. Lam, A. J. Qin, J. Z. Liu, Z. Li, B. Z. Tang, *Appl. Phys. Lett.* **2007**, 91, 3; b) Y. Hong, J. W. Y. Lam, B. Z. Tang, *Chem. Commun.* **2009**, 4332; c) J. Mei, Y. Hong, J. W. Y. Lam, A. Qin, Y. Tang, B. Z. Tang, *Adv. Mater.* **2014**, 26, 5429.
- [9] L. Xu, L. Jiang, M. Drechsler, Y. Sun, Z. Liu, J. Huang, B. Z. Tang, Z. Li, M. A. Cohen Stuart, Y. Yan, *J. Am. Chem. Soc.* **2014**, 136, 1942.
- [10] P. Cordier, F. Tournilhac, C. Soulie-Ziakovic, L. Leibler, *Nature* **2008**, 451, 977.
- [11] G. Schwartz, B. C.-K. Tee, J. Mei, A. L. Appleton, D. H. Kim, H. Wang, Z. Bao, *Nat. Commun.* **2013**, 4, 1859.
- [12] Z. Wu, R. R. Xue, M. Q. Xie, X. J. Wang, Z. H. Liu, M. Drechsler, J. B. Huang, Y. Yan, *J. Phys. Chem. Lett.* **2018**, 9, 163.